BOREAL ENVIRONMENT RESEARCH 20: 62–74
ISSN 1239-6095 (print) ISSN 1797-2469 (online)

Helsinki 27 February 2015

"O that awful deepdown torrent"

Peter Lundberg

Department of Meteorology/Physical Oceanography, Stockholm University, SE-106 91 Stockholm, Sweden

Received 13 June 2013, final version received 6 May 2014, accepted 19 Feb. 2014

Lundberg P. 2015: "O that awful deepdown torrent". *Boreal Env. Res.* 20: 62–74.

An overview of the deep-water flow from the Nordic Seas through the Faroe-Bank Channel and the Denmark Strait into the North Atlantic proper is given. These fluxes are of considerable importance for the global thermohaline circulation, and it is outlined how they can be modeled on the basis of rotating hydraulic theory for zero- as well as finite-potential-vorticity flow. The hydraulic framework is also shown to be useful for analyzing various dynamic features characterizing the deep-water flow.

Introduction

The immortal words from Molly Bloom's concluding soliloquy in *Ulysses* (Joyce 1924) reflected in the title of the present study pertain to the Atlantic-bound transport of warm and high-saline Mediterranean deep-water through the straits of Gibraltar. Similar deep-water fluxes of comparatively fresh (~34.9 psu) but very cold (~–0.5 °C), dense, deep water from the Nordic Seas take place through the Denmark Strait between Iceland and Greenland as well as through the Faroe-Bank Channel with threshold depths of 625 and 852 m, respectively. These are the two deepest passages through the Greeenland-Scotland Ridge, which delimits the deeper regions of the Nordic Seas from the North Atlantic proper (*see* Fig. 1), and hence play an important role as choke-points affecting the Atlantic Overturning Circulation (AOC) (cf. Dickson *et al*. 1990, Dickson and Brown 1994).

The overview of the Denmark-Strait and Faroe-Bank-Channel deep-water transports from the Nordic Seas to be given here is somewhat biased towards process studies in which the author has been directly engaged. For a broader perspective on the overflow problem in general as well as a global outlook, the reader is directed to the comprehensive review by Whitehead (1998).

The characteristics of the Denmark Strait and its importance as a possible "spillway" for the deep waters of the Nordic Seas was recognized already more than a hundred years ago when it was surveyed by Danish and Norwegian scientists (Mourier 1880, Knudsen 1899, Helland-Hansen and Nansen 1909). Although a few hydrographic surveys were undertaken in the 1920s (Defant 1930, Braarud and Ruud 1932), the first full-scale attempts to measure the volume transport of the overflow were not undertaken until the 1960s (Worthington 1969, Ross 1977, Ross 1984). Hereafter more-or-less continuous investigative work has been carried out in the passage, not least in conjunction with the World Ocean Circulation Experiment (WOCE) conducted in the 1990s (cf. Price and Baringer 1994, Käse and Oeschlies 2001).

As evidenced by the classical map of the Norwegian Sea (Fig. 2) due to Helland-Hansen and Nansen (1909), the presence of the Faroe Bank Channel was unknown at the turn of last

Editor in charge of this article: Kai Myrberg

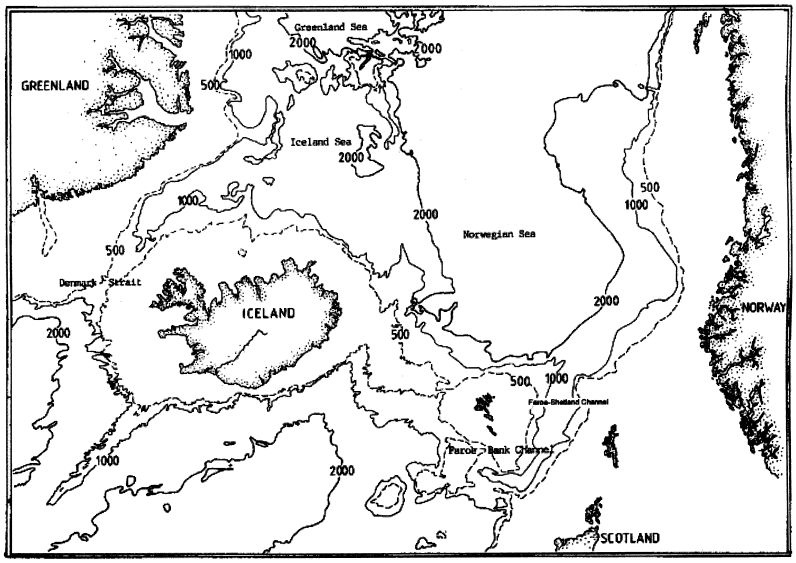

Fig. 1. The map of the Greenland–Scotland-Ridge area. The Denmark Strait between Iceland and Greenland as well as the Faroe-Bank Channel southwest of the Faroes are indicated.

Fig. 2. The map of the Iceland-Scotland-Ridge area as surveyed at the turn of the last century. Note that the Faroe-Bank Channel had not yet been surveyed. (from Helland-Hansen and Nansen 1909)

century. This passage was first discovered by the British in the early 1940s, when the Royal Navy maintained vessels equipped with echo-sounders in the area. The first hydrographic surveys of the passage were undertaken somewhat later (Cooper 1955, Dietrich 1956, Steele 1959), and in 1960 the International Council for Exploration of the Seas (ICES) organized the first multi-ship investigation of the deep-water overflow into the Atlantic (Crease 1965, Lee and Ellet 1968),

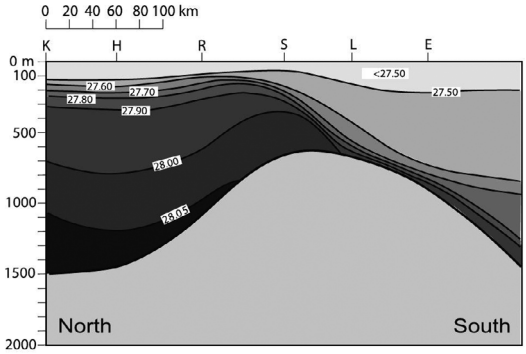

Fig. 3. Denmark Strait along-channel density transect. Note how the dense deep water after passage of the threshold moves southwards as a thin bottom layer. (from Nikolopoulos *et al.* 2003)

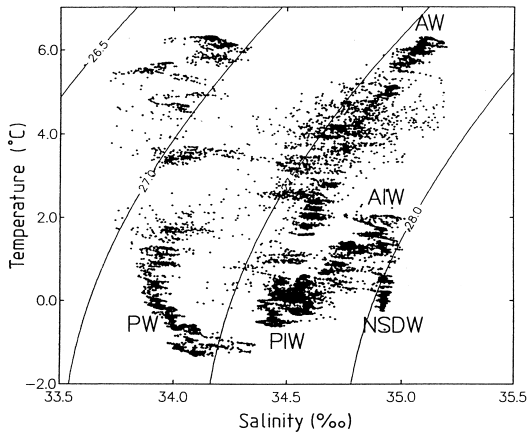

Fig. 4. The TS diagram from the Denmark-Strait threshold showing the presence of five distinct water masses.

an undertaking which was repeated in 1973 (Dooley and Meincke 1981).

Field investigations

Recent investigations of the deep-water overflows from the Nordic Seas have to a significant extent been undertaken within the Nordic-WOCE programme and its successors, i.e. mainly as a collaborative effort of Denmark, the Faroes, Finland, Iceland, Norway, Sweden, Germany, and Scotland, although note that United States research vessels have also played an important role in these field activities. In addition to periodic hydrographic surveys, a considerable part of the Nordic efforts was devoted to the maintenance of a number of arrays of Acoustic Doppler Current Profilers (ADCPs) as well as conventional recording current meters to monitor the surface- and deep-water fluxes across the Greenland-Scotland Ridge. For a review of the overall results of these investigations (cf. Hansen and Østerhus 2000). During the program, two 75-kHz ADCPs (both bottom-mounted in an upward-looking mode) were specifically dedicated to monitoring the deep-water transports through the Faroe-Bank Channel and the Denmark Strait at the thresholds of these passages. Additionally, three ADCPs were deployed across the Faroe-Bank Channel sill for a two-month period in the summer of 1998, this to establish estimates of the lateral variations of the deep-water flow here.

Conditions in the Denmark Strait

An along-channel snapshot of the Denmark-Strait overflow in the middle of August 1997 is shown in the longitudinal density transect in Fig. 3, where the high upstream-reservoir level of the "interface" separating the surface waters of Atlantic origin from the denser deep water emanating from the Iceland Sea is clearly seen. The TS diagram (Fig. 4) indicated that the hydrographic structure at the Denmark-Strait threshold is rather complex, this since the water column frequently comprises a number of different water masses: Norwegian Sea Deep Water (NSDW: 34.90 psu < S < 34.94 psu, T < 0 °C), Arctic Intermediate Water (AIW: 34.7 psu < S < 34.9 psu, 0 °C < T < 1 °C), Polar Intermediate Water (PIW: S < 34.9 psu, T < 0 °C), Atlantic Water (AW: S > 35.0 psu, 6 °C < T < 8 °C), and Polar Water (PW: S < 34.5 psu, T < 0 °C).

As recognized from two hydrographic sections worked by the r/v *Aranda* across the Denmark-Strait sill with a three-day interval (Fig. 5), the deep-water flux may vary considerably over shorter time-scales. This feature is also highly noticeable in long-term records obtained well downstream of the sill. The mechanism behind this variability is presently not fully understood (Smith 1976, Spall and Price 1998, Jungclaus *et al.* 2001, Käse *et al.* 2003); among other conjectures it has been suggested that it may be caused by an unstable barotropic surface jet (cf. Fristedt

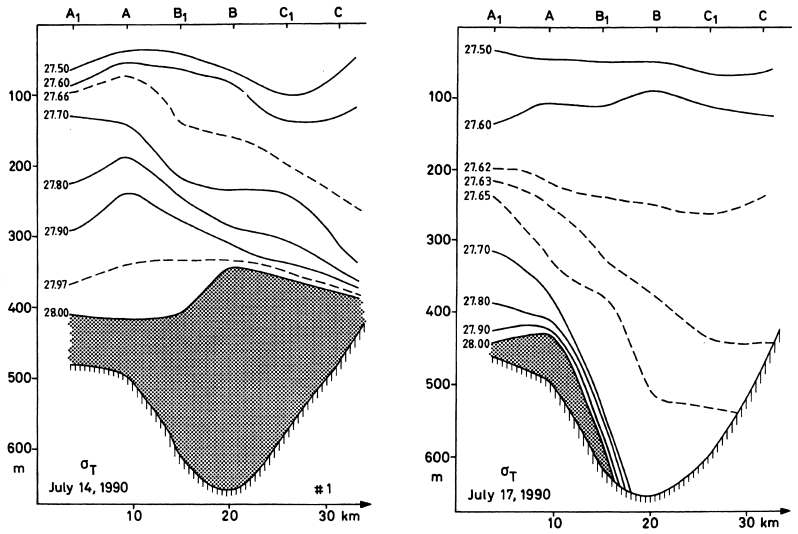

Fig. 5. Two cross-channel density sections at the Denmark-Strait sill taken with an interval of three days. Norwegian Sea Deep Water is represented by the cross-hatched area.

et al. 1999). Nevertheless, when estimating the transport over longer time-scales, the overflow has successfully been dealt with using rotating hydraulic theory (Nikolopoulos *et al*. 2003, Stern 2004, Macrander *et al*. 2005).

After transgressing the sill, the deep water moves southwestwards along the East Greenland shelf slope in the form of a thin bottom current, which as it widens assumes the form of a plume (Smith 1975). It deserves to be underlined that much of the research in the Denmark-Strait area has focused on the behaviour of this deep-water plume, which successively is entrained into the ambient water masses (Jungclaus and Backhaus 1994, Rudels *et al*. 1999, Girton and Sanford 2003), this since the overflow represents an important source term for the North Atlantic Deep Water.

Conditions in the Faroe region

In the Faroe area (cf. Fig. 6) the hydrographic conditions are significantly less complex than those encountered in the Denmark Strait. This region the hydrography is dominated by two distinct watermasses, *viz*. cold and low-saline Norwegian Sea Deep Water and warm Atlantic surface water of lower density (*see* Fig. 7). From this TS-diagram it should furthermore be noted that in the Faroe region the temperature may serve as a useful proxy for density, this due to the one-to-one relationship between salinity and temperature. Figure 8 thus shows three vertical profiles of the ADCP-recorded along-channel velocity as well as the simultaneously CTD-measured temperature. The stations denoted NWFC and NWFA were positioned on the southwestern and northeastern sides of the passage, respectively, whereas NWFB was located centrally in the channel. Note how the levels of maximum vertical shear coincide with those of the most pronounced temperature (i.e. density) gradients.

The overflow is known to be almost steady over shorter time-scales, and is at all times more-or-less geostrophically balanced (cf. Fig. 9 with examples of the sloping isotherm distribution across the passage). This feature can also be discerned from the temperature profiles shown in Fig. 8.

It should, however, be pointed out that the deep-water flux through the Faroe-Bank Channel shows a significant seasonality (Saunders 1990). Based on the Nordic-WOCE long-term ADCP records the transports have been found to vary between approximately 2.5 Sv (1 Sverdrup = 10^6 m^3 s^{-1}) in summer and 1.5 Sv during winter (cf. Fig. 10a). These transport estimates have been established on the basis of identifying the upper delimitation of the deep water with the level of maximum vertical shear and by also making use of the additional information on

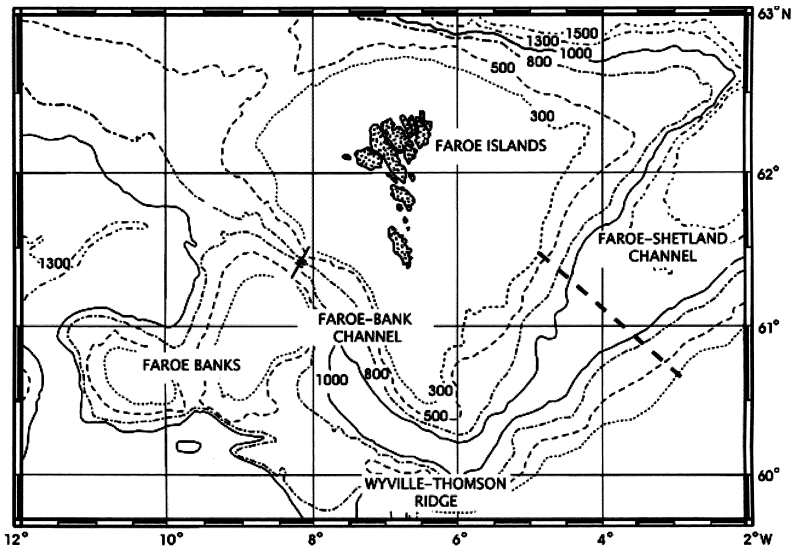

Fig. 6. Detailed map of the Faroe region. The solid line across the Faroe-Bank-Channel sill shows the standard hydrographic section where ADCP observations were obtained. The altimetric section across the Faroe-Shetland Channel is represented by the dashed line. (from Lake and Lundberg 2006)

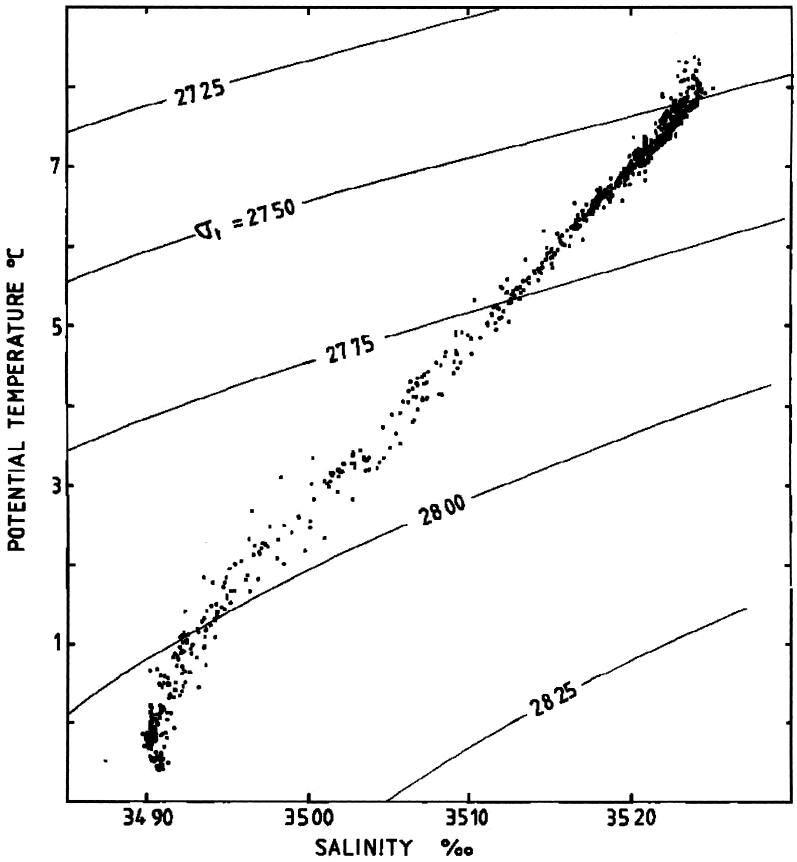

Fig. 7. TS-diagram from the Faroe region showing the presence of warm Atlantic surface waters and cold Norwegian Sea Deep Water. (from Borenäs and Lundberg 1988)

the lateral characteristics of the flow obtained during the two months in 1998 when three ADCPs were deployed across the threshold. Using satellite altimetry (SSALTO/DUACS), it proved possible to estimate the sea-surface-height (SSH) difference between the endpoints

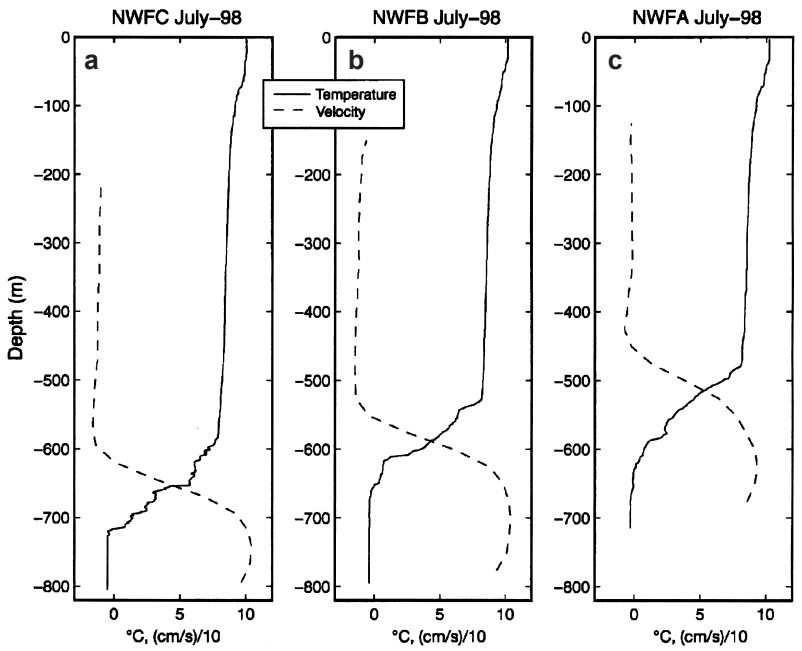

Fig. 8. Faroe-Bank Channel threshold profiles of temperature and velocity: (**a**) southwestern side of the passage, (**b**) the middle of the channel and (**c**) northeastern side of the passage. (from Lake and Lundberg 2006).

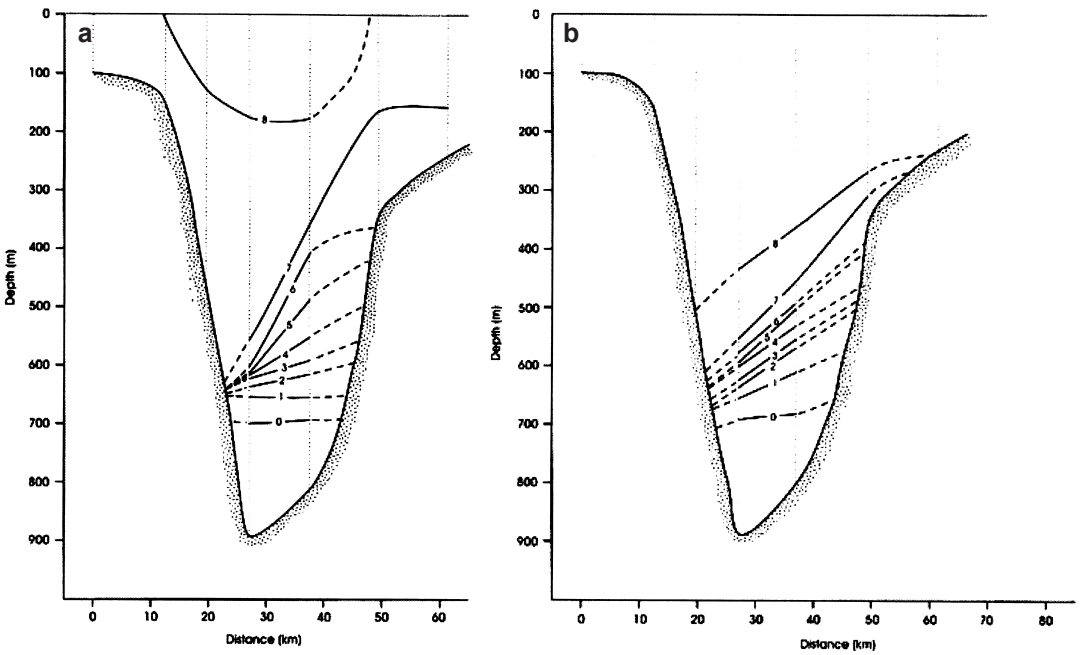

Fig. 9. Isotherm distributions across the Faroe-Bank Channel. (**a**) 17 May 1993: the most typical conditions, characterized by "isotherm pinching" on the southwestern side of the passage, and (**b**) 26 November 1991: isotherm distribution which is considerably more parallel. (from Borenäs *et al.* 2001).

of the dashed transect across the Faroe-Shetland Channel visible in Fig. 6. Using these altimetric results Lake and Lundberg (2006) showed that the seasonality is not due to changing upstream conditions in the Norwegian Sea, as erroneously inferred by Hansen *et al*. (2001). The variability

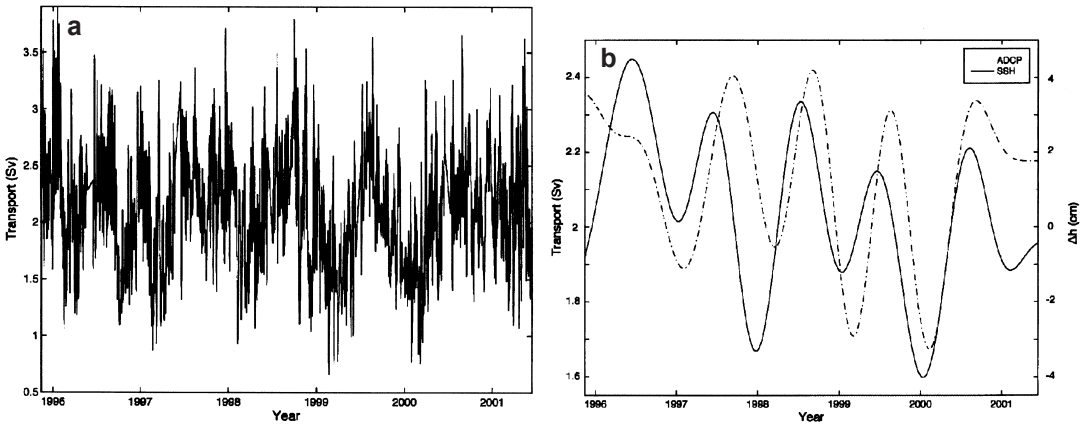

Fig. 10. (**a**) Daily averaged deep-water transports through the Faroe-Bank Channel 1995–2001. (**b**) The low-passed results also including the sea-surface-height (SSH) difference across the Faroe-Shetland Channel (solid line). (from Lake and Lundberg 2006).

is instead caused by the strong wintertime north-eastwards flow of Atlantic surface water through the Faroe-Shetland Channel. This surface flow, which primarily is wind-induced, is associated with an increased barotropic pressure gradient across the passage, which inhibits the geostrophically balanced deep-water transport south-westwards that feeds the Faroe-Bank-Channel overflow (cf. Fig. 6). Five-year records of the SSH difference across the Faroe-Shetland Channel and the observed deep-water transport across the Faroe-Bank Channel sill are shown in Fig. 10b. Both of these data sets have been subjected to Butterworth filtering with a 150-day low-pass cutoff. The altimetrically determined sea-surface slope across the channel is seen to lead the ADCP-determined transports by 1–2 months, *viz*. a lag consonant with the advective time scale characterizing the deep-water motion between the two observational sections.

Rotating hydraulic theory

As pointed out above, rotating hydraulic theory has proved useful for gaining an improved understanding of the dynamics of the deep-water flow through the Denmark Strait and the Faroe-Bank Channel. This conceptual framework, based on a two-layer approximation, assumes different guises depending on whether the flow is characterized by zero or finite potential vorticity (PV). The case of PV = 0 was investigated in a classical study due to Whitehead *et al*. (1974), who, however, postulated a rectangular passage. This approach can be generalized to a channel of parabolic shape, *viz*. $z = h(x) = \alpha x^2$, x being the cross-channel coordinate (cf. Fig. 11). (This bathymetry in many cases serves as a reasonable approximation of conditions encountered in nature; cf. Fig. 11b.) The interface separating the deep and quiescent surface waters from the lower active layer is located at $z = \eta(x)$, and the upstream-reservoir level of this interface above the threshold is taken to be η_∞. The along-channel velocity $v(x)$ is assumed to be geostrophically balanced: $fv(x) = g'\partial\eta/\partial x$, where g' is the reduced gravity and f is the Coriolis parameter. The inviscid flow is of zero potential vorticity: $(f + \partial v/\partial x)/[\eta(x) - h(x)] = 0$, and the fluid depth disappears at $x = -a$ and $x = b$. After a rescaling, $x = (g'\eta_\infty)^{1/2}f^{-1}x^*$, $v = (g'\eta_\infty)^{1/2}v^*$, $(h,\eta) = \eta_\infty(h^*,\eta^*)$, these equations can be combined into a second-order O.D.E., which, using the boundary conditions of zero fluid depth at the passage walls, has the solution

$$\eta(x) = -\frac{1}{2}x^2 + \frac{2+r}{2r}(b-a)x + \frac{2+r}{2r}ba, \quad (1)$$

where $r = f^2/(g'\alpha)$ and asterisks have been omitted. Introducing the averaging procedure

$$\langle\Phi(x)\rangle = \left[\int_{-a}^{b}\Phi(x)\,dx\right]\Big/(b+a), \quad (2)$$

the following quantities can be determined:

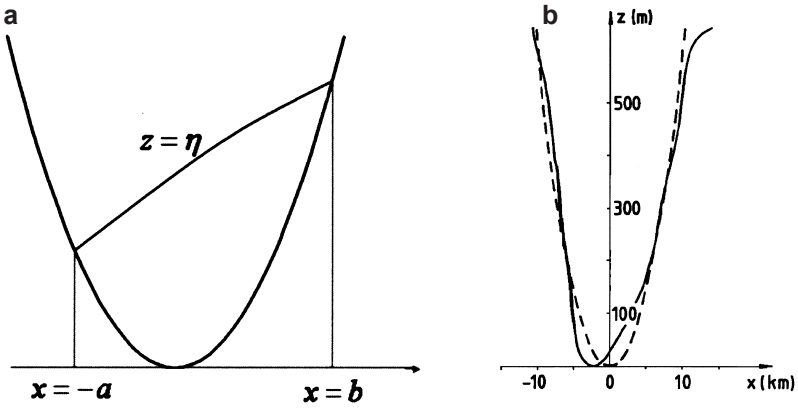

Fig. 11. (**a**) Idealized parabolic geometry including interface location. (**b**) Faroe-Bank Channel bathymetry (solid line) and its parabolic approximation (dashed). (from Borenäs and Lundberg 1988)

$$\langle v(x)\rangle = \frac{(b-a)}{r},$$
$$\langle v(x)^2\rangle = \frac{(b+a)^2}{12} + \frac{(b-a)^2}{r^2}, \quad (3)$$
$$\text{and } \left\langle \eta(x) - \frac{x^2}{r}\right\rangle = \frac{r+2}{12r}(b+a)^2.$$

Pratt and Whitehead (2007) showed that the Froude number F can be expressed as

$$F^2 = \frac{\langle v(x)\rangle^2}{\langle v(x)\rangle^2 - \langle v(x)^2\rangle + \left\langle \eta(x) - \frac{x^2}{r}\right\rangle} = \frac{6}{r}\frac{(b-a)^2}{(b+a)^2}. \quad (4)$$

Bernoulli's law $v(x)^2 + 2g'\eta(x) = 2g'\eta_\infty$, most conveniently evaluated at the passage midpoint $x = 0$, assumes the nondimensional form

$$\frac{1}{r}(b-a)^2 + \frac{1}{2}(b+a)^2 = \frac{4r}{2+r}, \quad (5)$$

hereby permitting the elimination of $b - a$ in the expression for the Froude number, which in the case of controlled flow, i.e. $F = 1$, yields $(b + a)_C^2 = 6r/(2 + r)$. Once this critical-flow width is known, Bernoulli's law yields $(b - a)_C^2$, and use can be made of the result for the nondimensional transport

$$Q = \int_{-a}^{b} v(x)\left[\eta(x) - \frac{x^2}{r}\right]dx = \frac{r+2}{12r^2}(b-a)(b+a)^3. \quad (6)$$

After insertion of $(b \pm a)_C$ and redimensionalization, the controlled transport is found to be

$$Q_C = \eta_\infty^2\left(\frac{3g'}{2\alpha}\right)^{1/2}\Big/(2+r). \quad (7)$$

This result is identical to that which independently may be obtained by maximizing Q (cf. Borenäs and Lundberg 1988). Conditions in the Faroe-Bank Channel are characterized by $g' = 4.3 \times 10^{-3}$ m s^{-2}, $\alpha = 5.8 \times 10^{-6}$ m^{-1}, $f = 1.27 \times 10^{-4}$ s^{-1}, and $\eta_\infty \approx 400$ m. This yields $r = 0.65$, and consequently the dimensional versions of the controlled transport and flow width are $Q_C \approx 2.0$ Sv and $(b + a)_C \approx 12\,500$ m, respectively, both in good agreement with observations.

To deal with the case of finite-PV rotating hydraulic flow through a passage is significantly more complex. The classical formalism describing this situation for a box-like channel is due to Gill (1977). His results were generalized by Borenäs and Lundberg (1986) to the same parabolic topography as dealt with above. For an upstream-reservoir depth D_∞ and a total transport Q, the problem proves to be governed by the following set of nondimensional algebraic equations for the intersection points $(-a,b)$ of the interface with the sloping walls of the passage:

$$a^2 = r - \frac{r}{\hat{D}_\infty^2}\left(\hat{\Psi}_i + \frac{1}{2}\right) - \frac{1}{2r}\left[(2+r)\tanh\left(\frac{a+b}{2}\right) - 2a\right]^2, \quad (8)$$

$$b^2 = r - \frac{r}{\hat{D}_\infty^2}\left(\hat{\Psi}_i - \frac{1}{2}\right) - \frac{1}{2r}\left[[2+r]\tanh\left(\frac{a+b}{2}\right) - 2b\right]^2. \quad (9)$$

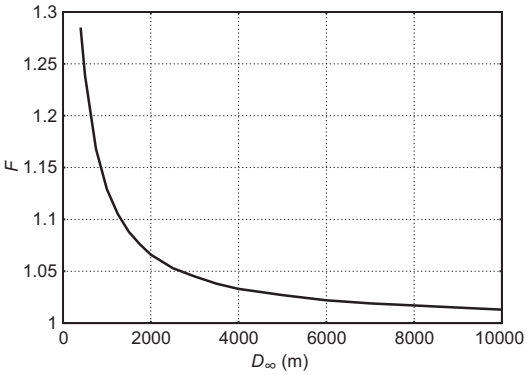

Fig. 12. Behavior of the finite-PV Froude number F as given by (10) for critical-flow condition at the Faroe-Bank Channel threshold as a function of the upstream-reservoir depth D_∞. It is seen that as the latter quantity increases, F approaches 1 as determined on the basis of zero-PV theory corresponding to an infinite upstream depth.

Here a and b have been scaled by $(g'D_\infty)^{1/2}/f$ and $\hat{D}_\infty = (g'/fQ)^{1/2}D_\infty$ is a nondimensional measure of the upstream-reservoir depth. The distribution of the volume flux between the side-wall boundary layers of this basin is specified by $\hat{\Psi}_i$, and the topographical parameter r is defined as above. For a discussion of the more subtle aspects of these equations as well as their derivation *see* Borenäs and Lundberg (1986). Provided that the parameters are prescribed such that flow over the threshold is permissible, the problem in general has two solution branches, one subcritical, the other supercritical. Controlled flow, implying maximum transport, takes place when only one solution exists, i.e. when the two branches merge. This state can be determined numerically, but additional insights are gained by dealing with Eqs. 8 and 9 using analytical techniques. Borenäs and Lundberg (1986) thus demonstrated how the problem could be resolved using a regular perturbative expansion based on the parameter $r^{1/2}$, in which case the lowest-order solution was found to be that for non-rotating hydraulic flow. Subsequently Laanearu and Lundberg (2005) introduced an analogous expansion based on $\hat{D}_\infty^{-1}$, for which the lowest-order result proved to be the zero-potential-vorticity solution discussed above. In both cases the governing equations required a preliminary rescaling before the problem could be dealt with using the series expansions.

As a corollary to their analysis of Eqs. 8 and 9, Borenäs and Lundberg (1986) showed that for finite-PV flow through a parabolic channel, the Froude number F assumed the following form:

$$F^{-2} = \left(\frac{\hat{D}_\infty}{r}\right)^4 (2+r)^2 \left[(a+b) - 2\tanh\left(\frac{a+b}{2}\right)\right]^2 \times \left\{\begin{array}{l} \left[a+b-(2+r)\tanh\left(\frac{a+b}{2}\right)\right]^2 \\ +2r(a+b)\coth(a+b) - 2r \\ -r(2+r)\tanh^2\left(\frac{a+b}{2}\right) \end{array}\right\} \quad .(10)$$

Although the analyses above for zero- and finite-PV flow differ fundamentally, the Froude-number results in the case of controlled flow can be compared, e.g. by using the dimensional zero-PV Faroe-Bank-Channel results for $(b + a)_C$ and Q_C as a baseline when evaluating the finite-PV Froude number (10). To do this, the flow width$(b + a)_C$ is rescaled based on D_∞, and the controlled transport Q_C is used for rescaling D_∞, whereas the bathymetric parameter $r = f^2/(g'\alpha)$ remains unchanged. Figure 12 shows how in this case the finite-PV Froude number is affected by a varying upstream-reservoir depth, and it is recognized that for an increasing D_∞, the Froude number approaches one, *viz*. precisely the zero-PV result.

Phenomenology of the Faroe-Bank-Channel deep-water flow

The framework of rotating hydraulics has proved to be useful for estimating the magnitude of deep-water transports, but can also be employed for gaining a deeper understanding of the dynamics of the flow. Enmar *et al*. (2009) thus applied the finite-PV Froude-number formalism to a year-long set of results from the Faroe-Bank-Channel long-term ADCP records. The Froude number proved to adhere very closely to its critical value $F = 1$ (cf. Fig. 13). This served as convincing evidence that the deep-water flow across the sill of this passage is controlled in the classical hydraulic sense, *viz*. that no signal emanating downstream of the control section can penetrate into the upstream reservoir. Figure 13a

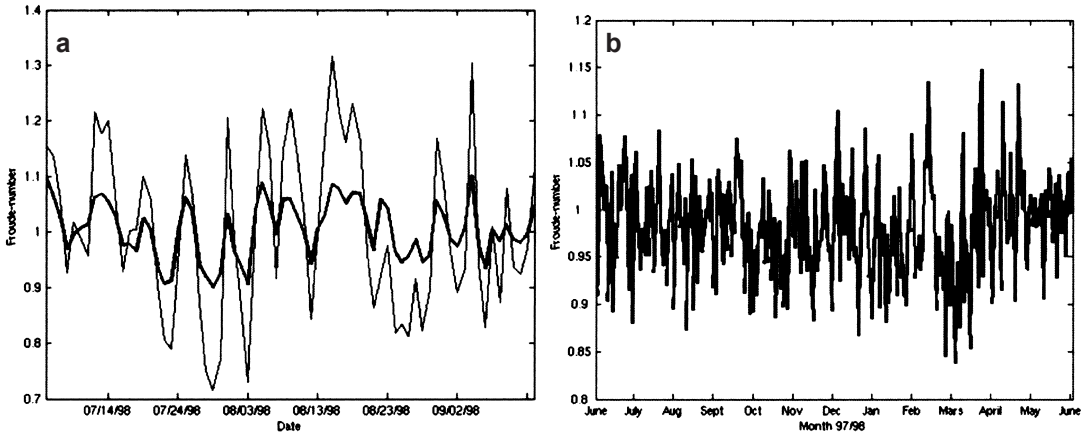

Fig. 13. (**a**) Finite-PV Froude numbers from the 70-day period with three ADCPs deployed on the sill. The weak line shows the results when the average flow during the period was used for scaling purposes, the heavy line when instantaneous transports were employed. (**b**) Froude-number results for a full year based on one centrally located ADCP. (from Enmar *et al.* 2009)

shows how the analysis is improved by utilizing instantaneous values of the transport (rather than the 70-day average) for scaling purposes.

Ever since hydrographic work at the threshold of the Faroe-Bank Channel started in the mid-1950s it has been noted that here the cross-channel distribution of isotherms frequently manifests a tendency towards "pinching" behaviour on the southwestern side of the passage (*see* Fig. 9a). Attempts have been made to explain this almost persistent feature as being due to cross-channel Ekman transports along the bottom as well as the interface separating the more-or-less passive surface waters from the rapidly moving deep water (cf. Johnson and Sanford 1992, Johnson and Ohlsen 1994). An alternative explanation advanced by Borenäs *et al*. (2001), based on previous results due to Hogg (1983, 1985), is that the overflow is not only constituted by NSDW, but also comprises an intermediate second water mass of slightly lower density, which, if its potential vorticity is conserved, yields precisely this "pinching" feature. Support for this conjecture is provided by the hydrographic cross-section shown in Fig. 9b, which demonstrates that pronounced pinching does not invariably occur. The composite TS-diagram (cf. Fig. 14) summarizes data from situations with pinching as well as without, and it may be recognized that for the pinched states the slight curvature of the upper cluster of TS-relationships indicates the presence of a third water mass constituted by North Icelandic Winter Water/Arctic Intermediate Water (NI/AI: 34.76 psu < S < 34.99 psu, 2.0 °C < T < 4.5 °C). This does not, however, rule out the possibility that cross-channel Ekman transports (which have been observed in the long-term ADCP records) also may play a role for maintaining this somewhat unusual hydrographic feature.

As previously noted, during a two-month period in the summer of 1998 three ADCPs were deployed across the Faroe-Bank-Channel threshold. The results from this intensive survey not only facilitated the establishment of highly precise transport estimates, but were also useful for examining the lateral homogeneity of the potential vorticity characterizing the deep-water flow. In view of the fact that the assumption of uniform PV is one of the cornerstones of rotating hydraulic theory, the appropriateness of applying this formalism to describe the Faroe-Bank-Channel deep-water flow could thereby be judged. Lake *et al*. (2005) showed that the deep-water potential vorticity manifested cross-channel variations (cf. Fig. 15), with the highest values found on the southwestern side of the passage. A detailed analysis revealed, however, that these variations were of too small a magnitude to impair the outcome of the maximal-flow predictions based on the assumption of constant and finite-PV critical flow at the Faroe-Bank-Channel threshold.

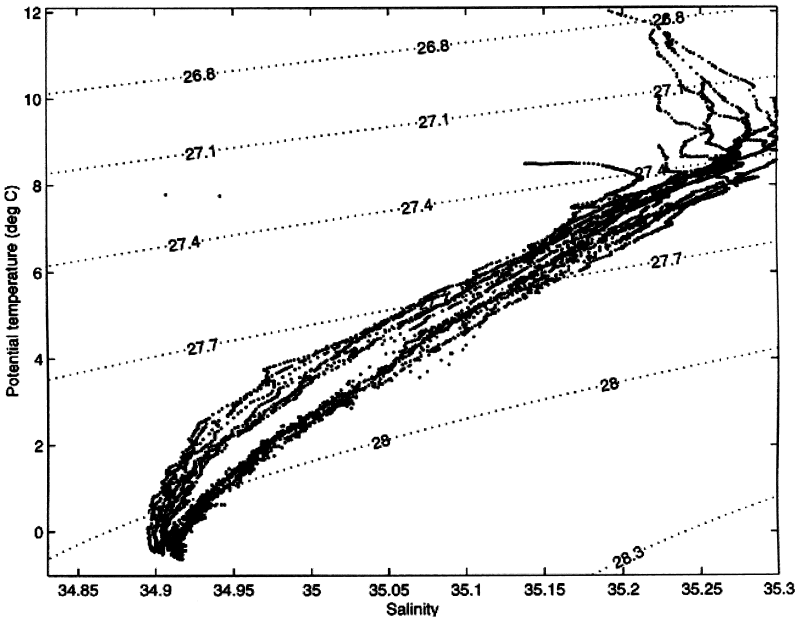

Fig. 14. Bimodal composite TS-diagram from the Faroe-Bank Channel. (from Borenäs *et al.* 2001)

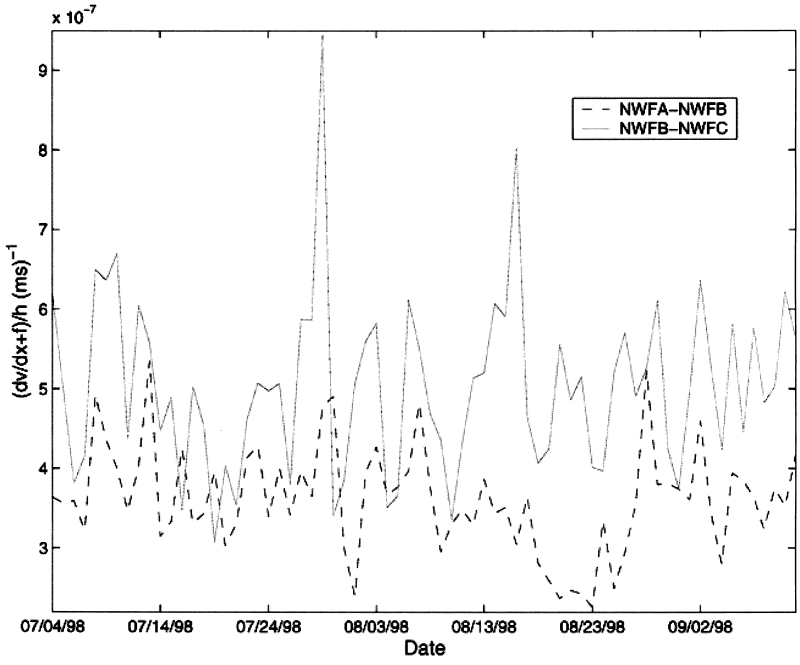

Fig. 15. Seventy-day evolution of the potential vorticity on the two sides of the passage. (from Lake *et al.* 2005)

Outlook

The overview of the deep-water flow through the Denmark Strait and the Faroe-Bank Channel given here has not dealt with the highly pertinent question of the role of these transports for the global thermohaline circulation. Investigations of this and related matters were first undertaken by Worthington (1970) in the late 1960s, and this general problem has ever since attracted considerable attention, most recently from Olsen *et al.* (2008).

An interesting process related to the Faroe-Bank-Channel deep-water overflow (which,

however, remains to be examined more closely) concerns the nature of signal propagation from the southern reaches of the Norwegian Sea to the sill region southwest of the Faroes. Does this take place in the form of a kinematic wave, as has been shown (Fristedt *et al*. 2002) to be the case in Öresund connecting the Baltic with the Kattegatt? During the Nordic-WOCE era an ADCP array was maintained across the Faroe-Shetland Channel, and the resulting long-term data set, used in conjunction with that from the threshold, should be highly useful when attempting to formulate an answer this question.

The present study may be concluded by noting how useful rotating hydraulic theory has proved to be when analyzing the large-scale overflows on the order of 10^6 m^3 s^{-1} across the Greenland-Scotland Ridge. The same has been shown to hold true for the Baltic Sea, where the saline deep-water originating from the Kattegatt and Skagerrak makes its way towards the interior basins via a series of constrictions and sub-surface conduits. A number of analyses based on rotating hydraulics (Laanearu and Lundberg 2003, Borenäs *et al*. 2007, Hietala *et al*. 2007) of these smaller-scale overflows (on the order of 10^4 m^3 s^{-1}) have been undertaken, all with remarkably successful results.

Acknowledgements: This work was undertaken with support from the Swedish National Space Board and the Knut and Alice Wallenberg Foundation. Altimeter products were made available by the CLS Space Oceanography Division as part of the EU ENACT project (EVK2-CT2001-00117) and with support from CNES. In addition to acknowledging the valuable assistance provided by Saeed Falahat as well as the constructive comments on a previous version of the manuscript by three anonymous reviewers, the author wishes to express his thanks to the crews and officers of r/v *Haakon Mosby* of Bergen and r/v *Aranda* of Helsinki as well as to his past and present co-workers K. Borenäs, L. Chafik, L. Enmar, T. Fristedt, R. Hietala, J. Laanearu, I. Lake, K. Lindblad, and A. Nikolopoulos.

References

Borenäs K. & Lundberg P. 1986. Rotating hydraulics of flow in a parabolic channel. *J. Fluid Mech*. 167: 309–326.

Borenäs K. & Lundberg P. 1988. On the deep-water flow through the Faroe-Bank Channel. *J. Geophys. Res*. 93: 1281–1292.

Borenäs K., Lake I. & Lundberg P. 2001. On the intermediate water masses of the Faroe-Bank Channel overflow. *J. Phys. Oceanogr*. 31: 1904–1914.

Borenäs K., Hietala R., Laanearu J. & Lundberg P. 2007. Some estimates of the Baltic deep-water transports through the Stolpe Trench. *Tellus* 59A: 238–248.

Braarud T. & Ruud J. 1932. The Øst expedition to the Denmark Strait 1929. *Hvalrådets Skr*. 4: 47–56.

Cooper L. 1955. Deep water movements in the North Atlantic as a link between climatic change around Iceland and biological productivity of the English Channel and the Celtic Sea. *J. Mar. Res*. 14: 347–362.

Crease J. 1965 The flow of Norwegian Sea water through the Faroe Bank Channel. *Deep-Sea Res*. 12: 143–150.

Defant A. 1930. Bericht über die ozeanographischen Untersuchungen des Vermessungsschiffes "Meteor" in der Dänemarksstrasse und in der Irmingersee. *Sitz. Ber. der Preuss. Akad. der Wiss. Phys. Math. Kl*. 16: 36–58.

Dickson R., Gmitrowicz E. & Watson A. 1990. Deep water renewal in the northern North Atlantic. *Nature* 344: 848–850.

Dickson R. & Brown J. 1994. The production of North Atlantic Deep Water: sources, rates and pathways. *J. Geophys. Res*. 99: 12319–12341.

Dietrich G. 1956. Überströmung des Island-Färöer-Rückens in Bodennahe nach Beobachtungen mit dem Forschungsschiff Anton Dohrn 1955/56. *Deutsch. Hydr. Z*. 9: 78–89.

Dooley H. & Meincke J. 1981. Circulation and water masses in the Faroese Channels during Overflow-73. *Deutsch. Hydr. Z*. 34: 41–55.

Enmar L., Borenäs K., Lake I. & Lundberg P. 2009. Comment on "Is the Faroe Bank Channel Overflow Hydraulically Controlled?". *J. Phys. Oceanogr.* 39: 1534–1538.

Fristedt T., Hietala R. & Lundberg P. 1999. Stability properties of a barotropic surface-water jet observed in the Denmark Strait. *Tellus* 51A: 979–989.

Fristedt T., Sigray P., Lundberg P. & Crona L. 2002. Salt-wedge observations in Öresund by direct measurements of the motionally induced voltage. *Cont. Shelf Res*. 22: 2513–2524.

Gill A. 1977. The hydraulics of rotating-channel flow. *J. Fluid Mech*. 80: 641–671.

Girton J. & Sanford T. 2003. Descent and modification of the overflow plume in the Denmark Strait. *J. Phys. Oceanogr.* 33: 1351–1364.

Girton J., Sanford T. & Käse R. 2001. Synoptic sections of the Denmark Strait overflow. *Geophys. Res. Lett*. 28: 1619–1622.

Hansen B. & Østerhus S. 2000. North Atlantic — Nordic Seas exchanges. *Progr. Oceanogr*. 45: 109–208.

Hansen B., Turrell W. & Østerhus S. 2001. Decrease of the overflow from the Nordic Seas into the Atlantic in the Faroe Bank Channel since 1950. *Nature* 411: 927–930.

Helland-Hansen B. & Nansen F. 1909. The Norwegian Sea. *Rep. Norw. Fish. Mar. Inv*. 2: 68–87.

Hietala R., Lundberg P. & Nilsson J. 2007. A note on the deep-water inflow to the Bothnian Sea. *J. Mar. Sys*. 68: 253–264.

Hogg N. 1983. Hydraulic control and flow separation in a multilayered fluid with applications to the Vema Chan-

nel. *J. Phys. Oceanogr.* 13: 695–708.
Hogg N. 1985. Multilayer hydraulic control with application to the Alboran Sea circulation. *J. Phys. Oceanogr.* 15: 454–466.
Johnson G. & Sanford T. 1992. Secondary circulation in the Faroe Bank Channel outflow. *J. Phys. Oceanogr.* 22: 927–933.
Johnson G. & Ohlsen D. 1994. Frictionally modified rotating hydraulic channel exchange and ocean outflows. *J. Phys. Oceanogr.* 24: 66–78.
Joyce J. 1922. *Ulysses*. Shakespeare and Co., Paris.
Jungclaus J. & Backhaus J. 1994. Application of a transient reduced gravity plume model to the Denmark Strait. *J. Geophys. Res.* 99C: 12375–12396.
Jungclaus J., Hauser J. & Käse R. 2001. Cyclogenesis in the Denmark Strait overflow plume. *J. Phys. Oceanogr.* 31: 3214–3229.
Käse R. & Oeschlies T. 2001. Flow through Denmark Strait. *J. Geophys. Res.* 105C: 28527–28546.
Käse R., Girton J. & Sanford, T. 2003. Structure and variability of the Denmark Strait Overflow: model and observations. *J. Geophys. Res.* 108C: 3181, doi:10.1029/2002JC001548.
Knudsen M. 1899. Hydrografi. *Den Danske Ingolf-expedition* 1: 76–94.
Laanearu J. & Lundberg P. 2003 Topographically constrained deep-water flows in the Baltic Sea. *J. Sea Res.* 49: 257–266.
Laanearu J. & Lundberg P. 2005. Analysis and improvement of a perturbative solution for hydraulic flow in a rotating parabolic channel. *Z. Angew. Math. Mech.* 85: 490–498.
Lake I., Borenäs K. & Lundberg P. 2005. Potential vorticity characteristics of the Faroe-Bank Channel Deep-Water Overflow. *J. Phys. Oceanogr.* 35: 921–932.
Lake I. & Lundberg P. 2006. Seasonal barotropic modulation of the deep-water overflow through the Faroe Bank Channel. *J. Phys. Oceanogr.* 36: 2328–2339.
Lee A. & Ellett D. 1968. On the contribution of overflow water from the Norwegian Sea to the hydrographic structure of the North Atlantic Ocean. *Deep-Sea Res.* 12: 129–142.
Macrander A., Send U., Valdimarsson H., Jónsson S. & Käse R. 2005. Interannual changes in the overflow from the Nordic seas into the Atlantic Ocean through Denmark Strait. *Geophys. Res. Lett.* 32: L06606, doi:10.1029/2004GL021463.
Mauritzen C. 1996. Production of dense overflow waters feeding the North Atlantic across the Greenland-Scotland Ridge; 1. Evidence for a revised circulation scheme. *Deep-Sea Res. Part 1* 43: 769–806.
Mourier A. 1880. Orlogskorvetten "Ingolf"s expedition I Danmarksstrædet 1879. *Geogr. Tidskr.* 4: 47–56.
Nikolopulos A., Borenäs K. Hietala R. & Lundberg P. 2003. Hydraulic estimates of the Denmark Strait overflow. *J. Geophys. Res.* 108C: 3095, doi:10.1029/2001JC001283.
Olsen S., Hansen B., Quadfasel D. & Østerhus S. 2008. Observed and modelled stability of overflow across the Greenland-Scotland Ridge. *Nature* 455: 519–523.
Pratt L. & Whitehead J. 2007. *Rotating hydraulics: nonlinear topographic effects in the ocean and atmosphere*. Springer, New York.
Price J. & Baringer M. 1994. Outflows and deep water production by marginal seas. *Progr. Oceanogr.* 33: 161–200.
Ross C. 1977. Preliminary results of recent overflow measurements in Denmark Strait. In: Dunbar M. (ed.), *Polar Oceans. Proc. Polar Oceanogr. Congr.*, pp. 99–106.
Ross C. 1984 Temperature–salinity characteristics of the 'overflow' water in Denmark Strait during 'OVERFLOW 73'. *Rapp. Proc. Verb. Reun. Explor. Mer.* 185: 111–119.
Rudels B., Eriksson P., Grönvall H., Hietala R. & Launianen J. 1999. Hydrographic observations in Denmark Strait in fall 1997 and their implications for the entrainment into the overflow plume. *Geophys. Res. Lett.* 26: 1325–1328.
Saunders P. 1990. Cold outflow from the Faroe Bank Channel: *J. Phys. Oceanogr.* 20: 29–43.
Smith P. 1975. A streamtube model for bottom boundary currents in the ocean. *Deep-Sea Res.* 22: 853–873.
Smith P. 1976. Baroclinic instability in the Denmark Strait overflow. *J. Phys. Oceanogr.* 6: 355–371.
Spall M. & Price J. 1998. Mesoscale variability in the Denmark Strait: The PV outflow hypothesis. *J. Phys. Oceanogr.* 28: 1598–1623.
Steele J. 1959. Observations of deep water overflow across the Iceland–Faroe Ridge. *Deep-Sea Res.* 6: 465–474.
Stern M. 2004. Transport extremum through Denmark Strait. *Geophys. Res. Lett.* 31: L12303, doi:10.1029/2004GL020184.
Whitehead J., Leetma A. & Knox R. 1974. Rotating hydraulics of strait and sill flows. *Geophys. Astrophys. Fluid Dyn.* 6: 101–125.
Whitehead J. 1998. Topographic control of oceanic flows in deep passages and straits. *Rev. Geophys.* 36: 423–440.
Worthington V. 1969. An attempt to measure the volume transport of Norwegian Sea overflow through the Denmark Strait. *Deep-Sea Res.* 16: 421–432.
Worthington L. 1970. The Norwegian Sea as a Mediterranean Basin. *Deep-Sea Res.* 17: 77–84.